universe

IMPACT FACTOR 2.9

CITESCORE 3.6

Article

Gravitational Quantum Mechanics —Implications for Dark Matter

Allan D. Ernest

MDPI

https://doi.org/10.3390/universe9090388

universe

MDPI

Article

Gravitational Quantum Mechanics—Implications for Dark Matter

Allan D. Ernest

Faculty of Science, Wagga Wagga Campus, Charles Sturt University, Wagga Wagga, NSW 2678, Australia; aernest@csu.edu.au

Abstract: The laboratory verification of the existence of gravitational eigenstates and studies of their properties in the Earth's gravitational field raises the question of whether the prediction of particle behaviour in gravitational wells would be any different if it were analysed using quantum theory rather than classical physics. In fact, applying Schrodinger's equation to the weak gravity regions of large gravitational wells shows that particles in these wells can have significantly reduced optical interaction cross sections and be weakly interacting compared to classical expectations. Their cross sections are dependent on their wavefunctional form and the environment in which they exist. This quantum phenomenon has implications for the dark matter (DM) problem. Analysis using gravitational quantum mechanics (GQM) has shown that a proton, electron, or any other particle within the standard model of particle physics (SMPP) could potentially function as a "dark matter particle" when bound in a gravity well, provided the gravitational eigenspectral ensemble of their wavefunction contains a sufficient proportion of the gravitational well's weakly interacting gravitational eigenstates. The leading theoretical paradigm for cosmic evolution, Lambda Cold Dark Matter (LCDM), currently lacks a suitable weakly interacting DM candidate particle, and gravitational quantum theory could provide a resolution to this. This article reviews the GQM approach to DM and provides some new results derived from the GQM analysis of particles held in the weak gravity regions of deep gravitational wells. It also outlines some predictions of the gravitational quantum approach that might be tested through observation.

Keywords: gravitational eigenstates; quantum theory; dark matter; neutron quantum states

Citation: Ernest, A.D. Gravitational Quantum Mechanics—Implications for Dark Matter. *Universe* **2023**, *9*, 388. https://doi.org/10.3390/universe9090388

Academic Editor: Antonino Del Popolo

Received: 27 July 2023
Revised: 21 August 2023
Accepted: 23 August 2023
Published: 28 August 2023

1. Introduction and Background

In 2002, Valery Nesvizhevsky et al. [1,2] first reported on an experiment carried out in the laboratories at the Institut Laue-Langevin in Grenoble, France. In this experiment, ultra-cold neutrons from the institute's reactor passed through a waveguide above a horizontal, mirror-like reflecting surface. During their travel, the neutrons were constrained in a vertical potential well bounded by a hard mirror-like surface below and the Earth's gravitational field above. What was found in this experiment was new and significant both for quantum theory and for gravity: Particles in gravitational wells form gravitational quantum eigenstates analogous to charged particles in Coulomb potential wells [1] [3,4]. From a quantum viewpoint, this observation is entirely expected, but given the lack of unification of general relativity (GR) with quantum mechanics (QM), many physicists had already concluded either that quantum theory does not apply to gravity outright or that quantum physics breaks down on large gravitational scales. Nesvizhevsky's experiments provide irrefutable proof that particles in gravitational potentials behave according to quantum rules, and so far, no large-scale limit to the validity of quantum physics has been observed. The behaviour of low-mass particles in gravitational wells, particularly their optical (electromagnetic) scattering cross sections, should be equally predictable from quantum theory.

In quantum analysis, the optical scattering cross sections of particles are predicted using QM applied to the weak gravity regions of these wells. It is assumed (as is generally the case in large wells) that particles remain bound before and after scattering and the unbound gravitational states are energetically inaccessible. Additionally, the theory does not consider scattering events in regions of strong gravity or in a scenario of quantized spacetime, as in [5–9]. The principal difference between bound–bound scattering amplitudes calculated in gravitational wells and free–free scattering amplitudes (such as Klein–Nashina Compton scattering calculations [10]) is that the sloping potential well spatially isolates weakly interacting gravitational eigenstates with significant energy differences from each other, whereas in the free–free case the eigenfunctions are always overlapping. This allows the bound states to remain optically isolated from other energetically distinct states in the well and provides a possibility for particles to become weakly interacting in these wells. Transition rates between non-spatially isolated states are also disfavoured because of the extremely low energy differences and so close that changes to a particle's wavefunction are physically negligible even after a multitude of transitions.

Importantly, despite the macroscopic nature of the eigenfunctions themselves and the spatial overlap of the of energetically close states, the narrow linewidth of the relevant states enables them to form a discrete energetically non-overlapping quantized set. In the outer region of a typical galactic halo the natural linewidth of long-lived states (where $n \sim 10^{33}$) is $\frac{\hbar}{\tau} \sim 10^{-40}$ eV (τ = state lifetime $\sim 10^{25}$ s), whereas the eigenstate separation ΔE is $\sim \frac{\mu G^2 m^2 M^2}{\hbar^2 n^3} \sim 4 \times 10^{-32}$ eV. Additionally, the eigenstate temporal periods in complex space are $\sim 10^{-15}$ s compared to typical free–particle–particle interaction times of halo gas particles $\gg 1$ s. The properties of localized wavefunctions (for example, Gaussian-type functions) representing pseudo-classical elementary particles can be calculated using the eigenspectral composition of the base gravitational eigenstates. It might be anticipated that quantum-derived photon scattering behaviour will yield the same results as those obtained from classical considerations, as expected from a quantum analysis of a baseball toss (historically the Correspondence Principle). But this is not to say that quantum physics will always predict classical outcomes [2] [11], and we should be prepared for the possibility that gravitational quantum mechanics (GQM) could lead to novel and unexpected effects.

GQM leads to an astonishing result: Ordinary elementary particles, when bound in the weak gravity regions of large gravitational halos, can exhibit significantly reduced optical interaction cross sections simply by virtue of their phase space location and their eigenspectral distribution, determined by their environmentally related wavefunction [12,13]. This should happen, possibly to a lesser extent, with other types of interactions as well. If this effect is sufficiently large, even stable, "normally visible" particles of the Standard Model could function as the weakly interacting massive particles (WIMPS) of the Lambda Cold Dark Matter (LCDM) theory or other dark matter particle theories. Thus, in GQM, particle darkness does not originate from the fundamental type of gauge boson mediating the particle's interaction but instead from the quantum rules of particle interaction in a bound structure (the gravity well) and involves the particle's quantum environment and eigenspectral composition. This quantum "environmental" darkness (so-called quantum dark matter or QDM) eliminates a need to invoke new physics or new particles beyond the standard model. This should be possible without significant modification to the relatively successful LCDM paradigm [14]. GQM may also be able to solve other observational conflicts of LCDM, including the "cusp" problem, the "satellite abundance" problem, and the "angular momentum problem." (See [15] for a review.)

This article is organized as follows. Sections 2 and 3 provide a review of previous work in GQM reported elsewhere [12–14,16–21]. They include a description of the mathematical procedure for interaction cross sections calculations and a discussion of the physical structure of the eigenstates that leads to them being "dark," as well as the trends in "particle darkness" with quantum parameters for simple systems [3]. Section 3 extends the GQM work of [12–14,16–21] and then presents new work reported at conferences of calculations of the eigenspectra of simple "toy model" Gaussian wavefunctions needing only a range

of low quantum-value eigenfunctions for their approximate description. The trends in particle darkness with quantum numbers seen in these simple wavefunctions suggest how GQM might solve some astrophysical problems, some of which are described in Section 4. Section 5 then offers a discussion of the formation of primordial halos in the early universe and in the scenario in which GQM would operate. It also discusses the need for reanalysis of Big Bang nucleosynthesis (BBN) and cosmic microwave background (CMB) anisotropy theory within the GQM context. Section 6 discusses some existing observational evidence for GQM and outlines observational tests of some of the predictions of GQM.

2. Mathematical Approach

2.1. Gravitational Potentials: Their Eigenstates and Eigenenergies

The demonstration of environmentally induced weak interaction of bound gravitational environments on a large scale can be carried out in a straightforward way using Schrödinger's equation applied to gravity [12]:

$$-\frac{\hbar^2}{2m}\nabla^2\psi + V(r)\,\psi = i\hbar\frac{\partial\psi}{\partial t}, \tag{1}$$

where m is the reduced orbit mass, $V(r)$ is the gravitational potential, and the other symbols have their normal meanings. In the case of a single central mass M and a small orbit (reduced) mass m, the potential $V(r)$ is $-GmM/r$, essentially a Coulomb-like potential.

A better approximation to real halo potentials is, of course, one that leads to flat rotation curves [16] and has a density profile of $\rho(r) \propto 1/r^2$. In this case, the potential has a logarithmic form $V(r) = -(GmM_0/R_0)ln(R_0\mathrm{e}/r)$ [16], where e is the exponential constant and R_0 and M_0 can be related to the virial parameters of the halo. Schrödinger's equation must be solved numerically in this logarithmic potential case.

Most investigations so far have been carried out using the simpler central point potential case (and it serves as a proof of principle of the effect). Simple schematic energy state diagrams for the central point mass potential (essentially a Coulomb-type potential for atomic hydrogen) and the logarithmic potential cases are shown in Figure 1, with energy increasing up the page. For the logarithmic potential, state energy increases with the quantum numbers n and l. The plotted purple and blue lines represent constant n and l, respectively. Each solid bar represents a set of $2l + 1$ degenerate m-valued eigenfunctions for each distinct (n, l) value. The $\Delta l = 1$ and $\Delta n = 1$ energy spacings for typical states in the outer halos of galaxies are of the same order (for $n \sim 10^{30}$, $\Delta E \sim 10^{-32}$ eV). We define a quantum parameter $p \equiv n - l$, which relates to the number of oscillations in the radial component of an eigenfunction and is the same quantum parameter $\nu = 1,\ 2,\ 3\ldots$ used in the atomic case, where angular momentum is included as part of a pseudo-potential [16].

2.2. Concept for Determining Optical Cross Sections of Halo Particles

The procedure for determining an effective optical cross section for a halo particle is as follows: The solution to (1) yields a base set of gravitational eigenstates $|u_i\rangle \equiv |u_{n,l,m}\rangle$ for a given potential. We do not expect that halo particles will be permanently in pure eigenstates. Even if a particle were in an eigenstate at a time t (say, because it had just undergone a radiative transition), collisions and temporal variations in the potential due to galactic processes mean that it would not be in an eigenstate for very long.

Any halo particle will have a wavefunction $|\psi\rangle$. The form of $|\psi\rangle$ is determined by our state of knowledge of the particle (Figure 2). $|\psi\rangle$ might be represented, for example, by a complex Gaussian wavefunction with a position centred on that of the particle and a packet speed (the Gaussian function's spatial oscillation frequency in complex space) determined by that of the halo temperature at the particle's position. We determine the Gaussian width (or spatial dispersion in phase space) from the particle's mean free path (related to the particle number density) and the momentum spread (variation in the Gaussian spatial oscillation frequency) from the spread in the Maxwellian distribution of speeds.

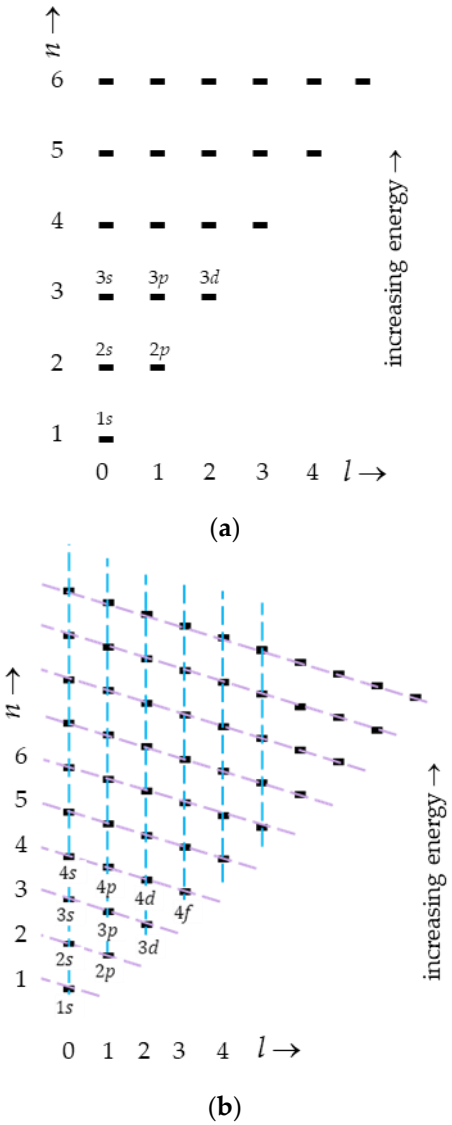

Figure 1. Simple schematic gravitational eigenstate diagrams for quantum numbers n and l (**a**) for the simplest $1/r$ Coulomb-like potential for a single central mass M_0 and (**b**) for a logarithmic potential arising from a $1/r^2$ radial mass density profile. (Each bar represents the $2l+1$, m-valued, z-projection sub-levels).

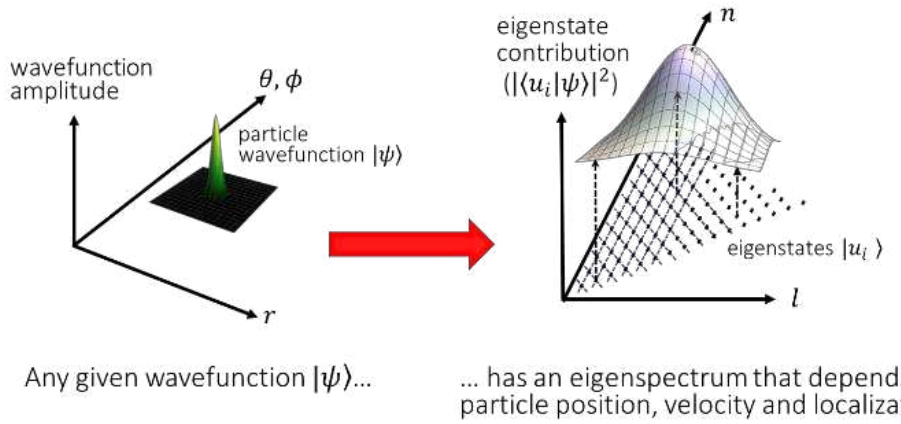

Figure 2. Schematic diagram illustrating the relation between a particle's wavefunction (in general, complex) and its eigenspectral amplitudes (also complex).

$|\psi\rangle$ can be represented by a weighted sum of the derived eigenfunctions $|\psi\rangle = \sum_i w_i |u_i\rangle$, whose weightings w_i are given by $w_i = |\langle u_i|\psi\rangle|^2$. In general, the cross section $\sigma_{particle}$ for any arbitrary interaction depends on the weighted sum of the individual cross sections σ_i for each of the separate eigenstates $\sigma_{particle} = \sum_i |\langle u_i|\psi\rangle|^2 \sigma_i$, where, again, $|\langle u_i|\psi\rangle|^2$ is the fractional contribution or weighting of $|u_i\rangle$ to $|\psi\rangle$ and $\sum_i |\langle u_i|\psi\rangle|^2 = 1$.

2.3. The Interactions of Photons with Wavefunctions

The present study involves the optical interactions of single photons with bound single particles in gravitational potentials. As noted above, the photon energy is such that the particle is gravitationally bound both before and after the scattering event, and the final and initial wavefunctions are assumed to be describable in terms of mixtures of bound gravitational eigenstates. The dark characteristics of halo particles arise through the relative differences in the structure, position, and range of the initial and final bound eigenstates in potential wells whose gradient decreases with radius [14,17]. This is very different behaviour to that calculated for spherical–square, finite, or infinite-sided potential wells [21] and for particles in field-free regions [10]. The cross section for a single photon scattering event involving a single localized Gaussian wavepacket is determined by the weighted sum of the state transfer probabilities per unit time over all the relevant eigenspectral component states on the state diagram. These are the Einstein B coefficients for state $|i\rangle$ to state $|f\rangle$, B_{if}, given by:

$$\begin{aligned} B_{if} &= \frac{\pi e^2}{3\varepsilon_0 \hbar^2 g_i} \sum_{m_i, m_k} |\langle m_k|\boldsymbol{r}|m_i\rangle|^2 \\ &= \left(\frac{c^3 \pi^2}{\hbar \omega_{if}{}^3}\right)\left(\frac{g_f}{g_i}\right) A_{if} \end{aligned} \tag{2}$$

where $B_{if} = \rho(\omega_{if})/P_{if}$, $\rho(\omega_{if})$ is the radiation energy density per unit angular frequency, $\langle f|e\boldsymbol{r}|i\rangle$ is the optical dipole matrix element for states $|i\rangle$ to $|f\rangle$, e is the electronic charge, ε_0 is the electrical permittivity, c is the speed of light, and $\hbar$ is Planck's constant. $\langle f|e\boldsymbol{r}|i\rangle$ is summed and averaged over the final $|m_k\rangle$ and initial $|m_i\rangle$ degenerate g_f and g_i states, respectively. A_{if} is the Einstein A coefficient [12,13], given by:

$$A_{if} = \frac{\omega_{if}^3 \, |\langle f|e\boldsymbol{r}|i\rangle|^2}{3\varepsilon_0 \pi \hbar c^3} \tag{3}$$

The probability of a photon of finite line width being scattered significantly on an entire journey across a potential well thus depends on the summation of the interaction rates for all available eigenspectral transition channels over all photon frequencies and Gaussian wavepackets representing all particles in the potential. The Einstein A coefficients are therefore of fundamental importance in determining the probability of bound–bound scattering events [12,13]. Particle–particle interactions can be similarly calculated with the relevant interaction Hamiltonians. In these cases, structural features still result in reduced cross sections, but it is not expected that the effect will be as great because of the more stringent angular selection rules in photon emission and absorption. The same arguments should apply to interactions of three bodies or more.

The high-n and high-l gravitational eigenstates in large-scale gravity wells have weak optical interaction because they have extremely low Einstein A coefficients with respect to virtually all energetically accessible states (Figure 3). Particles in these eigenstates have cross sections than the equivalent cross sections measured in a localized lab-based environment. Although somewhat analogous to the Rydberg states of electrons in atoms, the high (n, l) macroscopic gravitational eigenstates of the gravitational wells of galaxy halos have much greater binding energies, are more stable, and are longer-lived. It has been shown [12,13] that the higher the quantum number n is and the closer l is to n on the state

diagram in Figure 3, the darker and more weakly interacting an eigenstate is. Additionally, the number of states represented by each point on the state diagram in Figure 3 increases with l because of the degeneracy factor $(2l + 1)$. Indeed, the larger the structure, the more prevalent these dark gravitational eigenstates become as a fraction of the total available well-bound states. In the large gravitational wells of galaxy and cluster halos there is an overwhelming predominance of these well-bound, stable, dark states.

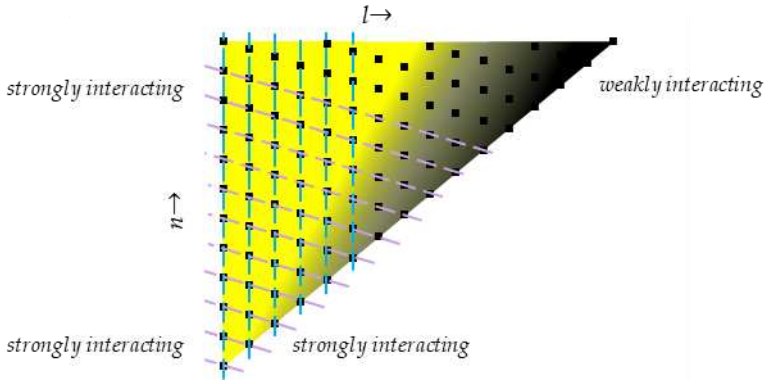

Figure 3. Schematic state diagram indicating qualitatively the relative variation in the interaction strengths of eigenstates (black squares) across the state diagram from strongly interacting (bright yellow) regions to weakly interacting (darkly shaded) regions.

As a general trend, therefore, the QDM effect increases with scale, as more dark states can potentially become incorporated into the particle's wavefunction (depending on the particle's wavepacket form and its position in phase space within the gravitational well). The specific darkness of any particle in a galaxy halo depends on (1) the distribution of its occupied states across the state diagram and (2) how the individual occupied eigenstate interaction rates vary with position on the state diagram. Both things can, in principle, be calculated using the formalism developed [12,13]. Because of the large quantum numbers involved, exact calculation of the degree of darkness is far beyond the scope of this manuscript. However, it is clear from current investigations (the results of which are still to be published) that approximate methods and trends can be developed and can be used to obtain accurate information on the average interaction rates of particles in a halo and hence the fraction of dark matter that a halo would appear to have. This highlights the need for extensive subsequent investigation into such calculations, and this is a primary consideration for our current and future research effort.

The scale at which GQM predicts a noticeable reduction in a particle's scattering cross section is clearly rather vague and depends on the eigenspectral composition of the wavefunction. At the scale of the Sun, the lifetimes of the highest high-n, $-l$ states are already of the order of hundreds of days, so it might be expected that dark storage of particles in the low-density corona environment beyond the chromosphere is feasible and could signify a detectable reduction in optical interaction cross sections beginning at this scale (high-(n, l) gravitational quantum states in the solar corona region have equivalent de Broglie kinetic energies similar to the corona temperature, and this may also explain how corona particles are trapped and maintained in the corona for long periods). A possibility exists for detecting the degree of reduced cross sections in the Sun's corona. The Sun is close enough that space probes travelling within the Sun's corona could directly measure the plasma density via in situ electron plasma resonance using a cavity (as is done by the Voyager probes—see Section 6.2) or via some other direct method. Such a measurement would yield particle densities unencumbered by any GQM-predicted reduced optical interaction of the individual particles. These density measurements could be compared with corona particle density measurements completed remotely via traditionally assumed Bremsstrahlung cross sections or other spectroscopic techniques. Calculating the exact theoretically expected difference in corona particle density using QDM versus traditional

Bremsstrahlung cross sections is beyond the scope of this manuscript (because of the quantum numbers involved) but should be calculable in the future using approximate methods to be developed.

2.4. Physical Properies and Structure of the Overlap Integral Leading to Weak Interaction

The low-p, high-(n, l) states have low A_{if} values because either (1) the energy difference between states and hence ω_{if} is small or (2) $\langle f|e\boldsymbol{r}|i\rangle$ is small. In situation (a) of Figure 4, the states have a significant overlap integral, but there is little difference in energy between the states and the frequency term in A_{if} is small. In (b), the frequency becomes significant, but by this stage the states are spatially disjointed and the overlap integral is zero. In (c), in states where the energy is substantial, there are vast differences in the spatial oscillation frequencies (SOFs) of the initial and final states and, again, the overlap integrals become negligible [14,17]. For binary optical interactions, the angular momentum selection rules associated with $\langle f|e\boldsymbol{r}|i\rangle$ further restrict transitions involving interactions in the low-particle-density regions of halos, as only $l = \pm 1$ transitions can take place.

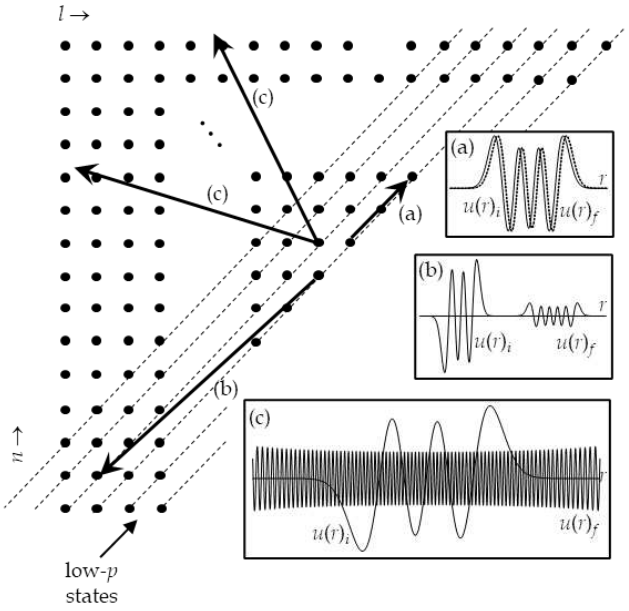

Figure 4. The structure of radial eigenstate component functions, showing the various physical reasons for weak interaction properties of (high-n, l), low-p states), Ernest [14]. In cases like (a) the overlap integral is not negligible but the energy difference is close to zero. In cases like (b) the initial and final eigenfunctions are spatially disjoint and the overlap integral is essentially zero. In cases like (c) there are vast differences in the SOFs.

The physical reason why particles in field-free regions do not exhibit the same degree of quantum environmental darkness is that in field-free regions eigenstates always overlap and spatial separation of highly differing energy states never occurs. Particles in wells with vertical walls also always have overlapping states. Spherical potential wells whose potential gradient function $f(r)$ decreases with r are uniquely able to produce weakly interacting eigenstates. Overlapping integrals in these gradient wells that involve $p = 1$ states are essentially zero, even for overlapping states with $p \gg 1$.

3. Calculation of Cross Section Trends for Simple Systems (Low n, l)

The rationale for studying simple systems is as follows: The aim of GQM is to calculate interaction rates for various two-body interaction processes in the low-density environments of macroscopic gravitational systems. The quantum representation of particles in macroscopic gravitational systems involves extremely large quantum numbers. It is essential, therefore, to develop methods for calculating interaction cross sections for eigen-

states with arbitrarily large values of quantum numbers applicable to this environment. Future calculations for these large-scale environments will be approached by two methods: (1) developing mathematical procedures for approximating overlap integrals with high spatial oscillation frequencies and (2) developing formulae for trends that can be used to accurately extrapolate interaction rates across the state diagram for both particle–radiation interactions and particle–particle interactions. Additionally, it has been shown [12,13] that some interactions for the highest l-valued states can be calculated directly for arbitrary values of n. These calculations will provide a check on the accuracy of the extrapolation procedures.

For now, in this section, the results of calculations carried out on some simple gravitational quantum systems are presented. The two factors influencing the darkness of a halo particle are the darkness of the individual eigenstates in its eigenspectral composition and the fractional contribution they make to the particle's packet wavefunction. Section 3.1 contains the results of the calculations of trends in the interaction cross sections (Einstein A coefficients) carried out for simple toy systems ($n < 100$). These results show the variation in eigenstate darkness across the state diagram for constant n. Section 3.2 provides the absolute value of the eigenspectral contributions needed to form simple Gaussian wavepackets with various radial positions and momenta. These provide an intuitive feel for how a reduction in Einstein A values comes about because of the shift in the eigenspectral distribution into dark or visible regions of the state diagram and how wavepacket shape and phase space position influence the degree of darkness.

3.1. The Variation of Cross Section/Einstein A Coefficients across the State Diagram

The quantum numbers of the eigenstates in an actual galaxy halo can be very large. The darkest states in the top right-hand corner of Figure 3 have n and l values of typically $\sim 10^{30}$. The eigenfunctions can, in general, have an intractable number of terms in their functional forms. For the states along, or very close to, the right-hand diagonal of Figure 3, however, $p = 1$, and there are approximate formulae for A_{if} for any optically allowed state ($\Delta l = \pm 1$) involving them. Ernest [12,13] derived an approximate formula for A_{if} for transitions where one state is on the right-hand diagonal. For high $-(n, l)$ states in a typical Milky Way-sized halo, the Einstein A coefficients can be typically of the order of 10^{-25} s^{-1}, corresponding to a lifetime many orders of magnitude greater than the age of the universe. As a result, these states are totally invisible, unable to transfer to other positions across the state diagram either electromagnetically or gravitationally, and are therefore unable to participate in gravitational coalescence and facilitate any scattering processes (such as Compton scattering).

In [12,13], Ernest considered the rate of stimulated scattering of high $-(n, l)$ states by various types of halo radiation, including the cosmic microwave background, stray visible starlight, and Thomson, Rayleigh, and Compton scattering. In each case, the scattering rate of the high-(n, l) states is so small that it can be considered negligible. These states have no optical way of transferring to the more strongly interacting region of the state diagram, and to do so would require the (still feeble) particle–particle interactions or three-body mechanisms, which are extremely rare in the outer halos of galaxies.

Photon-induced optical transition cross sections, appropriate to galactic halo particles, could also be investigated by calculating and extrapolating empirical scaling relationships for smaller (n, l). Because A_{if} is a proxy for optical absorption and scattering cross sections, relative state-to-state cross section trends can be obtained directly from A_{if} values. Figure 5 shows how the relative cross section varies with l and n across the state diagram for low n and l [18]. The ratio of the optical absorption cross section for the darkest ($l = n - 1$) to the most visible ($l = 0$) transition is strongly dependent on the value of n and l and on the size of the quantum jump Δn. Of importance for dark matter is how significantly the dark-to-visible state-to-state absorption cross section ratio is reduced when one moves to galaxy halo scales ($n \sim 10^{30}$, for example, corresponding to average radii in the outer Milky Way) and one considers optical frequency transitions ($\Delta n \sim 10^{21}$). In this case, the

ratio of the least visible (high l, low p) to most visible (low l, high p) state transitions (for $n \sim 10^{30}$) is $\sim 10^{-10^{21}}$ [12,13], making particles with significant fractions of high $-(n,l)$ states in this region potentially extremely dark across most of the electromagnetic spectrum.

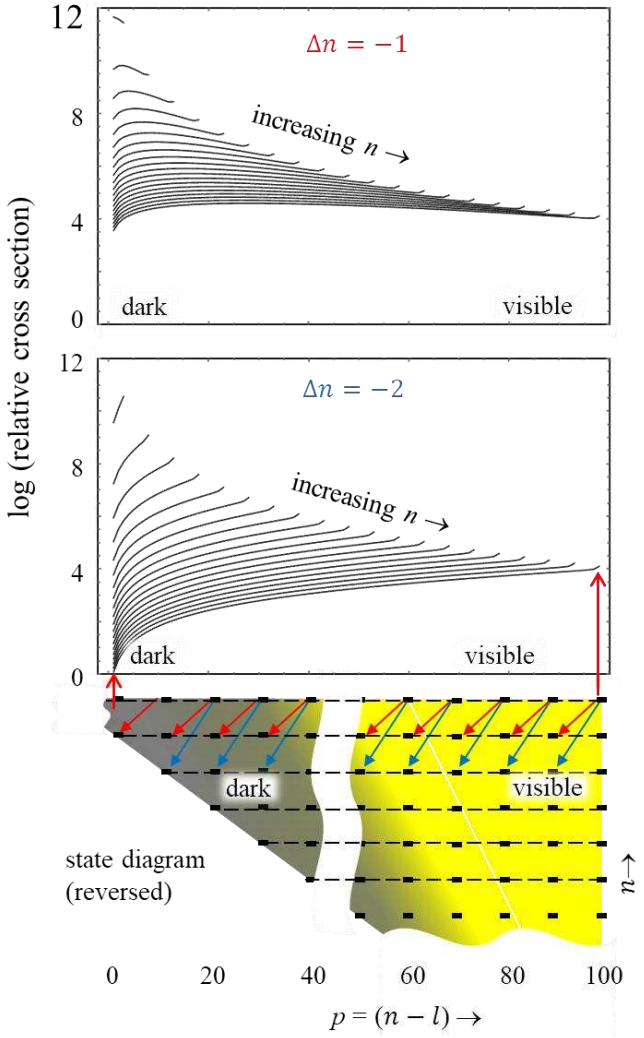

Figure 5. Variation of Einstein A coefficient (A_{if}, ∝ state-to-state absorption cross section) with n and l for low values of n and $l < 100$ for a Coulomb-type potential. The red arrows correspond to $\Delta n = -1$ and the blue arrows to $\Delta n = -2$. Note that, here, for $\Delta n = -2$, the highest l states are about 10^4 times more weakly interacting (i.e., darker) than the most visible states. For $\Delta n \sim 10^{21}$, values equivalent to optical frequencies in the halo, this relative darkness factor is $10^{10^{29}}$ (Whinray and Ernest [18]).

Whinray and Ernest [18] also found a relation between the net state lifetime τ and the (n,l) value of a state $\tau \propto n^3 l^2$. Since this net state lifetime originates from the inverse of the sum of the decay rates to multiple allowed decay channels, it still fixes an upper limit to the value of A_{if} for any individual channel that provides upper limits to any high-(n,l) state visibility.

3.2. Wavefunction Eigenspectra and Particle Properties in Toy Models

A greater fraction of dark eigenstates in a particle's eigenspectrum leads to more DM-like properties. The aim here is to investigate how the eigenspectral distribution is affected by the wavefunction and environment. The figures in Figure 6 show the calculated absolute values of eigenfunction contributions to various Gaussian toy model wavefunctions. Because these calculations are computationally intensive, parameters of the so-called toy halo

potential wells and Gaussian wavefunctions have been chosen here so that the significant (n, l)-value eigenspectral contributions are <100. These toy models can be used to predict qualitative trends. The variables of the Gaussian wavefunction investigated include radial position in the halo and particle radial velocity. Figure 6a shows that Gaussian wavefunctions (particles) that are further out in a halo and in larger halos have larger dark eigenstate contributions and greater potential for darkness. Figure 6b compares the eigenspectrum of stationary particles with those moving radially. A particle with a larger radial velocity has relatively less angular motion and therefore fewer high-l (dark) and more low-l (visible) eigenstates in its eigenspectrum, which means it interacts more. Despite the very small values of n and l, there is no reason to suspect that the trends shown here should not be extendable to real halos.

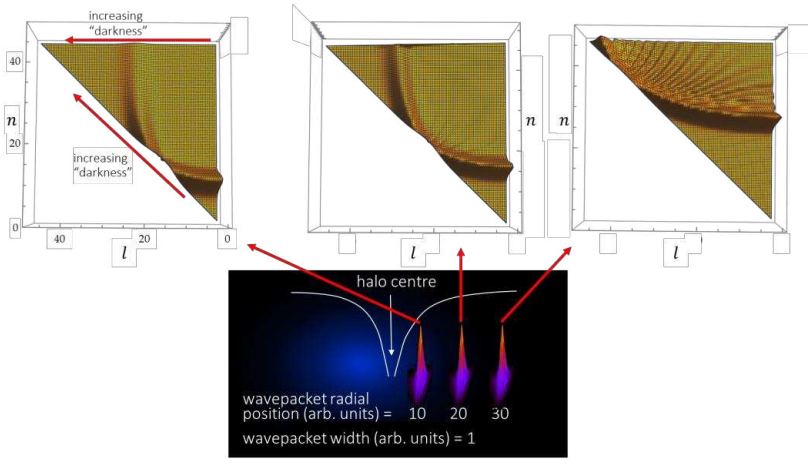

(**a**)

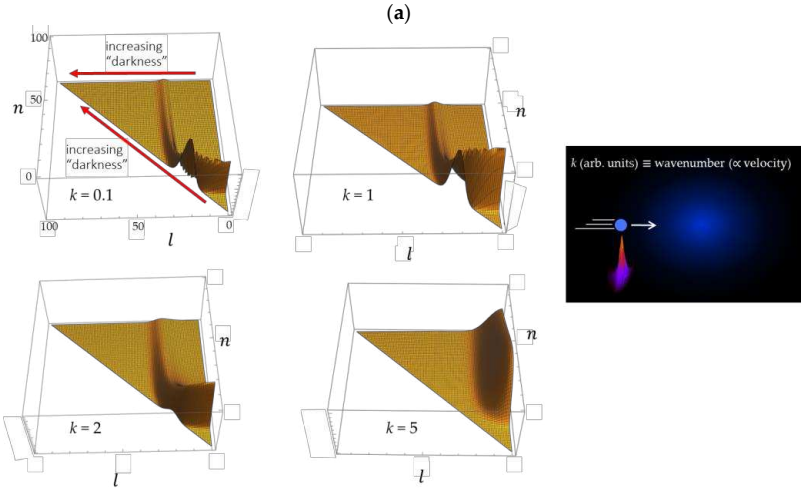

(**b**)

Figure 6. Schematic diagrams showing 3-D plots of calculated absolute values of the relative contributions of eigenfunctions across the (n, l) state diagram to Gaussian-type wavefunctions with low-quantum-value (low (n, l)) eigenspectra (<100) in a simple simulated toy model $1/r$-type potential. The vertical axis is a measure of the probability that a particle with a given Gaussian wavefunction occupies a given (n, l) $(m = 0)$ state. No allowance has been made in these calculations yet for m degeneracy, which obviously increases with l value. (**a**) When a particle is further out from the potential centre (Gaussian centre = 10, 20, 30 and the Gaussian width (arbitrary units), its eigenspectrum contains a greater fraction of dark states (shifts to darker, higher (n, l) regions). (**b**) The effect on the eigenspectral composition of radial motion. When a particle has a higher radial velocity (either moving inwards or outwards and achieved by incorporating a Gaussian function of the form $e^{-ikx+(r-r0)^2/4\Delta r^2)}$, where k is the wavenumber relating to the particle momentum via the de Broglie relation), the eigenspectral distribution shifts to a more highly visible ensemble of eigenstates.

4. Consequences for Astrophysics

4.1. Particle Radial Density Profiles in GQM

Each value of (n, l) comprises a set of $(2l + 1)$ m-degenerate eigenstates that, taken together, form a spherically symmetric radial probability density distribution. Maxwell–Boltzmann statistics provide the probabilistic relative occupancy of the (n, l) levels at equilibrium. Binning and summing the corresponding eigenstate probability density functions leads to a scale-invariant radial mass density profile $\rho(r) \propto 1/r^2$, as shown in Figure 7, as approximately observed in most galactic rotation curves. Note that a logarithmic potential does not necessarily imply that an inverse square density would be predicted at equilibrium.

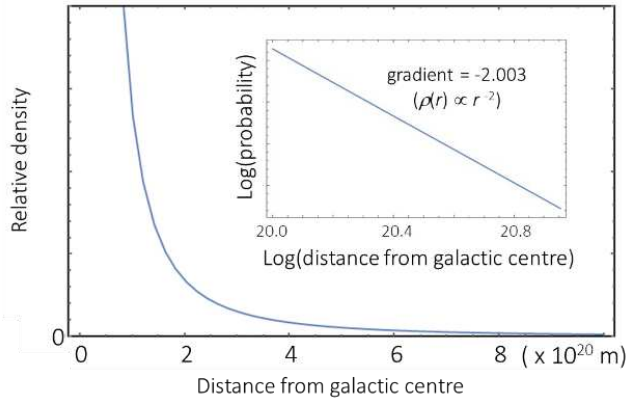

Figure 7. Binning and summing the equilibrium state population probability densities leads to $1/r^2$ scale-independent radial density profiles.

4.2. Darkness Fraction and Equilibrium; Significance for Star Formation and Quenching Rates

Two factors tend to increase the fraction of dark eigenstates in a halo particle's eigenspectrum with the approach to equilibrium: One is that the occupancy of dark, high-l states is favoured by the fact that eigenstate energies decrease with increasing l, and two, the dark high $-(n, l)$ states have high degeneracies ($\propto 2l + 1$). Thus, as equilibrium is approached, the contribution of dark states to the galactic halo wavefunction increases, the halo becomes less visible, and the particles become less interactive, resulting in an increase in the effective dark matter fraction of the halo. Isolated halos equilibrated through particle–particle coupling (though still weak) can be shown to have a less visible halo ensemble of states, which leads to a reduction in available star-forming material. When merger events occur, however, particle radial velocity components can be relatively increased. Figure 6b shows what happens to the particle eigenspectrum—it shifts to a more active regime with more visible states. In addition to infalling gas, weakly interacting, non-coalescing star-forming material is already there; merging shifts baryons into more highly interactive states that can participate in usual star formation processes. On the other hand, isolated halos slowly evolve toward less interactive equilibrium wavefunction ensembles with subsequently less star formation. This shows how quantum theory provides an additional mechanism for the ebb and flow of star formation in galaxy halos.

4.3. How Eigenstate Spatial Oscillation Frequencies Affect Interactivity in Galaxy Halos

When the spatial oscillation frequencies of the initial and final eigenstates differ markedly, the overlap integrals are significantly reduced, and interaction cannot take place as effectively [22]. The qualitative effects that de Broglie wavelength differences have on the size of the overlap integrals and the degree of interaction can be seen in the jets of streaming particles from galactic centre black holes. De Broglie wavelengths of the emitted particles close to the black hole are extremely small but decrease with radial distance as the jet particles slow down while travelling against the direction of the gravitational field. Eventually, their wavelengths are close enough to the surrounding halo baryons

and interaction becomes more likely. In the same way, the so-called jellyfish galaxies leave extended trails or "tentacles" of star formation, when the de Broglie wavelength/velocity of the halo particle and host cluster halo is favourable for particle interaction.

4.4. Globular Clusters and Dwarf Spheroidal Galaxies: A Common Primordial Ancestor?

LCDM predicts many more dwarf satellite galaxies than are observed. The situation is closer to being resolved if globular clusters are included in the count of dwarf satellite galaxies. GQM provides a mechanism to enable globular clusters (GC) to be part of the satellite galaxy population. In GQM, the conjecture is that GCs and dwarf spheroidal (dSph) galaxies are the direct descendants of the same primordial halo objects. Both contain evidence of one or more central massive black holes, as expected if they were the same types of objects. However, dSphs are the most dark matter-dominated structures known, whereas GCs have little to no DM. At first sight, this would suggest that they are objects with very different origins. How is the dark matter difference resolved in the GQM conjecture?

It is asserted in the GQM scenario that the baryonic halos of dSphs have been largely undisturbed since their original formation (apart from star formation). Left alone, these baryonic halos have equilibrated so that their overall eigenspectral ensemble is dominated by dark eigenstates (as discussed in Section 4.2), making them some of the most dark matter-dominated structures in the universe.

Globular clusters are, however, speculated to have had a very different history by virtue of having had considerably more interaction with their host galaxies by having orbits that passed around and through the discs or halos of their large host galaxies. With each pass through a halo, weak particle–particle interactions shift their baryons into more highly interacting eigenspectral compositions (Figure 6b), resulting in the gravitational coalescence of gas and a burst of star formation. Once a GC has left the densest part of the host halo, the remaining uncoalesced gas re-equilibrates, and the cycle repeats on each halo pass until most of the baryons have been converted to stars. In this way, we observe GCs to have little dark matter but still contain massive central PBHs, like dSphs. We thus predict GCs to be associated with larger galaxies or galaxy cluster halos and to be predominantly composed of ancient stars, with possibly two or more stellar generations. Lone GCs far away from other galaxies or galaxy cluster structures should not be common, whereas lone dSphs would be more likely. This scenario predicts that the long-term averaged radial positions of a galaxy's GCs will be less than that of its dSphs. This has been seen to be the case for the GCs and dSphs of the Milky Way and M31 [20].

5. The GQM Scenario for Halo Formation—Primordial Black Holes from the e^+/e^- Phase Transition and Their Relation to Galaxy Number Density

Particles with dark eigenspectral ensembles form naturally in large gravitational wells. Ernest (2003) [23] suggested that if GQM was correct it would imply a need for the formation of supermassive primordial black holes in the early universe. It was predicted that these black holes should be $< \sim 10^{36}$ kg at formation and that they can be found today at the centres of galaxies of all sizes and at the centres of globular clusters [23]. Although controversial at the time, the evidence for these supermassive black holes has grown [24], and it is now reasonably well established that they exist in the centres of most galaxies. These primordial supermassive black holes provide deep wells to enable the capture formation of baryonic material in the form of dark eigenspectral ensembles and explain how a universe can be all baryonic yet still be consistent with the two pillars of evidence that originally led to the hypothesis that dark matter is composed of a particle beyond the standard model. The two pieces of evidence are the predictions from BBN [25] and an analysis of the CMB anisotropies [26]. Strong evidence from measurements of the light element abundances as predicted from BBN and analysis of the CMB anisotropy observations implies that baryonic matter makes up at most only about one fifth of the total matter content. GQM does not claim that the observational data are wrong but suggests that the theoretical basis of these observations needs reformulation in a universe where

gravitational quantum mechanics implies that the cross sections used may be in error in the environment of bound gravity wells [14,16]. In the GQM scenario, such deep gravity wells would form as a result of direct collapse during phase transitions in the early universe [27–31]. This enables the existence of dark eigenspectral ensembles before recombination and even at or before BBN [32]. One possible scenario [14,23] to achieve this is further discussed below. Even at the earliest times, LCDM modelling of early cosmic evolution such as in [33] needs to be formulated against the backdrop of a universe scattered with the potential wells of black holes with masses over several ranges, corresponding to their formation at each of the phase transitions that enabled their production.

It is well known theoretically that the production of primordial black holes (PBHs), with masses up to approximately the horizon mass, is possible in over-density regions at various phase transitions in the early universe [25,27]. At the $t \sim 1$ s, e^+/e^- phase transition, this corresponds to PBH masses of $\sim 10^{35} - 10^{36}$ kg. Ernest [16,23], in discussing the early halo formation scenario in GQM, suggested that galactic centre black holes should be of at least this mass and possibly a lot greater, with a primordial origin that originated from this particular phase transition. By applying Carr's PBH number density relation [25] to the $t \sim 1$ s phase transition, it is possible to obtain an order of magnitude estimate of the present-day equivalent number of such supermassive black holes. This number density is similar to the present-day number density of galaxies [14], although the estimate is dependent on the equation of state softness parameter, as discussed by Carr [25], and what is taken as a merger rate over cosmic history. Nevertheless, the equivalence is intriguing. Furthermore, recent observations of galaxies formed very early that are now being observed by the James Webb Space Telescope [24,34] suggests that these supermassive primordial black holes from the electron–positron phase transition are a necessity for such early formation of the galaxies.

The gravitational potential around $t \sim 1$ s phase transition PBHs is significantly deeper than the thermal energy of the particle–radiation background at the time for a considerable distance out from the PBH. Even without the formation of weakly interacting eigenspectra, the radiation–particle collision processes cannot prevent halo formation near these very massive PBHs at or before BBN [14]. Protons and electrons can be gravitationally held in these PBH wells, even without the possibility of weakly interacting eignespectral compositions. As time proceeds, the surrounding cosmos cools and expands, increases the contrast density, and enables further capture as the PBH–halo gravity field travels outwards. The GQM-predicted reduced scattering cross sections add to the potential for capture. A simplistic model [14] shows that quite massive halos can form before the completion of BBN, with masses limited only by the presence of adjacent halos. This early halo formation enables much earlier structure formation and differs from standard LCDM, where baryon capture occurs later, after DM halo formation. In the GQM scenario, the size and number of primordial baryonic halos are inversely related and depend on the number of over-density regions and on the value of the softness parameter in the Carr number density equation [14]. Hence, an estimate of the number density of equivalent pre-merged galaxies in the universe should yield information about the conditions at the $t \sim 1$ s phase transition time.

Supermassive black hole formation by direct collapse would be expected to be accompanied by the emission of gravitational waves. We would expect that if virtually all of the supermassive black holes found at galactic centres were of primordial, direct collapse origin, then the universe should be filled with the gravity wave noise of these collapse processes. The gravity wave spectrum should reflect the number density and size of these $t \sim 1$ s black holes and the black hole mass spectrum, calculable from [25]. The recently suggested detection of super-long wavelength gravitational waves using pulsar timing [35] may be evidence for such a direct collapse. At $t \sim 1$ s, the supermassive black holes of the GQM scenario should produce gravitational waves of wavelengths of the order of the gravitational waves seen since the $t \sim 1$ s horizon distance ($r_h \sim 3 \times 10^8$ m) multiplied by the $t \sim 1$ s redshift factor ($z \sim 2.7 \times 10^9$) $\approx 8 \times 10^{18}$ m.

In the QDM scenario, the $t \sim 1$ s direct collapse black holes and their primordial halos are in place at a very early time [14]. This results in severe inhomogeneity during the BBN process, much more than has been assumed so far in the literature. Preliminary (unpublished) work on this using the density variations expected from primordial halo formation, with the standard BBN elemental abundance prediction curves, suggests that inhomogeneity alone may be sufficient to allow for a baryonic universal density fraction of $\Omega_B \sim 0.3$. This suggests that a reanalysis of BBN that includes the reduced BBN cross sections different from those obtained in reactor measurements, but potentially predictable from GQM theory inside primordial halos, is also necessary. Such reanalysis could lead to a final deuterium abundance consistent with what is currently measured but for a greater original baryon-to-photon ratio (η_{10}). It may also help with the lithium problem [36], as the abundance curves for lithium-7 and lithium-6 versus η_{10} have opposite gradients around the expected η_{10} value.

An Important process in the formation of CMB anisotropy is that of baryon acoustic oscillation (BAO) [31,37], which is critically dependent on the Compton scattering cross section from free electrons. Ernest [14] discussed the possibility that, at decoupling, pre-existing halos were so close that there may have been only small regions between halos that could be considered field free. In this case, the Compton scattering process takes place predominantly in the bound halo wells, where the scattering cross section is much reduced. No theory of BAO in a region of space containing such a high concentration of halo wells has yet been investigated. The number density of halo wells at decoupling (equivalent to the present galaxy number density evolved back to $z \sim 1100$) corresponds to $l \sim 20,000$, so anisotropy relating to individual halo well number density will not be directly observable in the anisotropy power density spectrum.

6. Observational Tests and Predictions from GQM

6.1. Dark Matter Fractions of High-Temperature Halos

No direct evidence of a dark matter particle has been observed. The possibility that a dark matter particle may simply be a consequence of a particle's environment and quantum history is attractive because it does not require a particle beyond the standard model. But how is the existence of a particle wavefunction with a predominantly dark eigenspectrum verified? We cannot specifically distinguish the detection of a proton with such a wavefunction from one with a more highly visible eigenspectrum. Its detection would simply be a proton, and its presence would not be unexpected, because gravity would suggest that it existed there anyway. Additionally, it would not necessarily carry any history of its pre-detection wavefunction. A better test of GQM is to make GQM predictions about halo composition and dark matter fractions and compare them with observations. The GQM prediction is that the DM-to-gas mass ratio would be larger for large structures with less interaction history [14,19] and that equilibrated structures might have observed DM-to-gas mass ratios that vary in a predictable way with scale (Figure 6a).

Observationally, the DM fraction of a galaxy halo is determined by adding together the galaxy's stellar and gas mass components and subtracting this "visible" mass from the dynamical mass, as determined from observations of rotation curves and lensing. One possible test is to use the procedure of Section 3 to better determine the true mass of the gas component using the predictions of GQM. The eigenspectral distribution of the halo particle wavefunctions is estimated from the wavefunction quantum interaction history, mean free path, velocity, and associated uncertainties. Theoretically, by calculating the GQM eigenstate interaction cross sections for all combinations of eigenstates in the halo well, the in-situ cross sections for all processes and particles in the halo can be obtained under any conditions. These theoretical data can then be used to recalculate the GQM-based estimate of the galaxy's gas mass. The stellar plus revised GQM-calculated gas mass can then be compared to the dynamical mass of the galaxy as before and used to determine whether exotic dark matter is still required. It is well known that large spiral and elliptical galaxies and clusters of galaxies have very hot ($10^6 - 10^8$ K), almost totally

ionized halos [38]. Calculating halo mass using GQM-derived cross sections is probably the only way to get a true measure of the halo density and determine whether the total eigenspectral ensemble of particles (plus stars, black holes, etc.) will match the observed dynamical mass.

6.2. GQM Predictions for Low-Tempertaure Halos: HI-Dominated, Dark Matter-Free Galaxies, and H_2-Dominated, High-Dark Matter Galaxies

Perhaps the most definite test to explain the nature and origin of dark matter from GQM comes from observations of low-temperature halos. In particular, the recently discovered dark matter-free galaxies and dark matter-dominated low-temperature halos will provide outstanding observational testing grounds. Not all halos are hot, and lower-temperature halos may be composed of compound particles with an internal structure such as HI or H_2. Absorption or emission of radiation from the internal transitions in these species will yield an accurate measurement of their number density because the cross sections for internal processes are not dependent on the gravitational eigenspectra of the wavefunction itself. Thus, for low-temperature halos where there is little to no HI, it is possible to obtain an accurate mass of the halo gas component provided the temperature is known.

The Doppler dispersion σ_T of the internal gas transition linewidths provides a direct measurement of the gas temperature of an equilibrated halo. Caution is needed, however, because any observed galaxy dispersion σ_{obs} includes the bulk rotation and other motions of the halo gas as well as the internal dispersion of the transition linewidths. Additionally, observed velocity dispersions are usually line-of-sight or radial measurements $\langle v_r^2 \rangle$—that is, $\sigma_{obs}^2 \equiv \langle v_r^2 \rangle = \frac{1}{3}\langle v_{total}^2 \rangle$ [39]. The halo's M_0/R_0 ratio (see Section 2) yields the bulk rotation speeds of stars and gas using the enclosed mass $M_0 r/R_0$ and $\frac{mv_r^2}{r} = \frac{GM_0 r}{R_0 r^2}$, respectively, but can also provide an approximate upper limit on the gas temperature, assuming that the gas temperature can be related to the average eigenfunctions' de Broglie wavelengths. In GQM, eigenstates have an equivalent kinetic energy, as determined by the eigenfunctions' de Broglie wavelengths when averaged as per the virial theorem. Assuming that the σ_{obs} can serve as providing an approximate upper limit to these de Broglie wavelengths, M_0/R_0 can be used to yield an estimate of a halo's temperature. In virtually all astrophysical situations, this yields at least one order of magnitude of agreement with measured halo temperatures, ranging from the largest clusters of galaxies to dwarf galaxies, the Sun's corona, and the Earth's ionosphere [19]. For an equilibrated halo, the mass M_0, size R_0, and effective concentration (M_0/R_0) of an equilibrated halo can then be related to the fractional phase composition of HII, HI, and H_2. Importantly, GQM predicts that the variation in M_0/R_0, ratios, the associated gas temperatures, and proximity to equilibrium give rise to a large range of observed dark matter fractions, ranging from halos that are virtually dark matter free to ones that are dominated by dark matter. Of course, a galaxy could appear to have no dark matter simply because it has little to no gas whatsoever (like most GCs and galaxies like the relic galaxy NGC 1277 [40,41]). In GQM, however, a low-temperature halo could have substantial gas content and appear either dark matter free, if it was almost all HI (detected by, say, 21 cm radiation), or dark matter dominated, if it was not in equilibrium or contained large fractions of H_2.

For equilibrium conditions and halo particle densities of $10^6 - 10^7$ m^{-3}, the Saha equation provides the 50% dissociation temperature ($H_2 \leftrightarrow 2$ HI) between 900 and 1100 K, depending on density and other factors. Similarly, the range of ionization temperatures (HI $\leftrightarrow$ HII + e$^-$) is between 3000 and 4000 K. There is a narrow range of temperatures between dissociation and ionization where an equilibrated and necessarily quiescent galaxy halo could consist almost entirely of atomic hydrogen. GQM predicts that such HI-rich and HII- and H_2-deficient galaxies would then appear to be dark matter free. Dark matter-free or almost dark matter-free galaxies are expected to be rare because there are many processes that could result in a galaxy being contaminated with potentially dark HII or H_2. The halo must contain a large diffuse (HI) gas component, it must be in a high degree of equilibrium,

and it must have a tightly constrained M_0/R_0 ratio. Its equilibrium temperature must lie in the narrow range required for HI dominance ($1 - 3 \times 10^3$ K), and lastly, it must be quiescent and isolated so that there is little production of HII or H_2 from ongoing internal processes or from external infall. Although rare, such quiescent, HI-rich, dark matter-free galaxies have recently been observed—for example, the ultra-diffuse galaxy (UDG) AGC 114905 [42]. For an equilibrated, virialized halo with an inverse square radial density profile, the halo temperature T relates to the observed face-on, radial HI velocity dispersion σ_r via $T \sim m_{HI}\,\sigma_r^2/k$, where k is the Boltzmann constant. The HI dispersion value in AGC 114905 is ~ 5 km/s, implying an equilibrium halo temperature of ~3000 K, a halo temperature in the range where almost all hydrogen could be present as HI. Significantly, AGC 114905's halo also has far more HI than expected for a typical galaxy. This excess of HI in AGC 114905 is equivalent to a situation where all the dark matter of standard LCDM had been replaced with atomic hydrogen. Other UDFs with halo velocity dispersions that suggest that they could have HI-dominant halos and be dark matter free include NGC1052-DF2 ($\sigma_r \sim 7.8 \pm^{5.6}_{2.2}$ km/s) and NGC1052-DF4 ($\sigma_r \sim 4.4 \pm^{4.2}_{2.2}$ km/s).

There are many even smaller halos in the universe with lower masses and lower M_0/R_0 ratios (e.g., dSphs). The existence of these galaxies whose halo temperatures, as per their velocity dispersions, could be considerably lower than AGC 114905 suggests a further observational test for GQM. These galaxies generally have a very high dark matter content. If their halos are in equilibrium, their lower M_0/R_0 ratios mean that their halo temperatures could be low enough that the halo composition may include, or even be dominated by, hydrogen in the molecular phase. Examples include ultra faint galaxies such as Segue 1 and Segue 2. These galaxies are considered some of the most DM-dominated galaxies in the universe. GQM, however, predicts that the dark matter observed in these dwarf galaxies is molecular hydrogen. Molecular H_2 does not emit 21 cm radiation, and so it is not surprising that the H_2 has gone undetected and been interpreted instead as the (dominant) dark matter component of the halo. It is proposed that efforts be put into the detection of this molecular hydrogen. Currently, H_2 densities are deduced using CO as a proxy. This proxy is known to be unreliable [43], and the transfer rate between CO and H_2 is likely be problematic, according to GQM. H_2 would be detectable via emission of radiation from rovibrational transitions of the molecule and, as already mentioned, the flux of this radiation will only depend on temperature and *will not* be affected by the gravitational eigenspectral distribution of the H_2 molecule itself. Hence, according to GQM, if the total mass of the H_2 in these halos can be accurately measured using this radiation, then the halo should show no mass deficit. The emission of rovibrational radiation depends on the gas temperature (via $T \sim m_{HI}\,\sigma_r^2/k$) and the degree of excitation of the rovibrational energy levels, and these need to be deconvoluted. Possible candidates include Hydrus I ($\sigma = 2.7 \pm 0.5$ km/s), Reticulum II ($\sigma_* = 3.3 \pm 0.7$ km/s), Carina II ($\sigma = 3.4 \pm^{1.2}_{0.8}$ km/s), and Segue I ($\sigma = 3.7 \pm^{1.4}_{1.1}$ km/s) [44,45]. Infrared and microwave radiation from this rovibrational radiation may be detectable via the James Webb Space Telescope if the halo temperatures are suitable. Another way of measuring the H_2 mass without using a proxy is to look for absorption of the molecular Lyman–Werner lines from radiation passing through the low-temperature halos. This, of course, requires a continuum source such as a background quasar directly behind the dwarf galaxy. Both observations need the temperature of the halo known to a high degree to determine the H_2 number density. Specifically, the GQM prediction is that these low-temperature, super dark matter-dominated halos will be composed almost totally of molecular hydrogen. Provided the mass of that molecular hydrogen can be measured accurately by JWST or by background quasar Lyman–Werner line scattering, this molecular hydrogen should make up the shortfall in the mass of these galaxies and eliminate the need for exotic dark matter, just as was found for the dark matter-free galaxies that contained principally atomic hydrogen.

6.3. Other Evidence for Excess HI?

There are two recent observational results that hint at excess hydrogen atoms in the universe. The first comes from the EDGES experiment [46], designed to study the

epoch of reionization (EoR) in the early universe. The experiment detected a 78 MHz absorption feature, corresponding to red-shifted 21 cm HI radiation originating at $z = 17$. The significance of the result is in the amplitude of the signal, which was considerably greater than expected and could be interpreted as indicating a much greater concentration of atomic hydrogen in the early universe than theory predicts. Several other suggestions have been put forward for why the signal is so much larger than expected, but further observations are needed to establish the origin of the discrepancy.

The second result comes from the Voyager space probes that are believed to now be beyond the heliopause of the Solar System and in a position to make in situ electron density measurements of the interstellar particle number density. This direct particle number density measurement uses electron plasma oscillations in a cavity. These density measurements show an increase in electron density beyond the heliopause that is greater than expected, 0.12 $cm^{-3} \pm 15\%$ [47,48], compared to theoretical predicted values of ~0.3 $\sim$ 0.03 cm^{-3}.

7. Discussion and Summary

The physics behind GQM is straightforward and sound: We now have experimental proof that (1) particles exist in gravitational quantum states formed in gravitational potential wells and (2) current experiments have entangled wavefunctions spanning hundreds of kilometres, and it is expected that there will be no limit to the scale at which QM can be used to predict particle behaviour and properties. GQM is not a theory but a prediction based on these two aspects of physics. The optical cross sections of the interaction of photons with particles (scattering and emission) are predicted to be significantly reduced in large-scale gravitational wells of galaxy halos when compared to what might be expected from measurements made in Earth-based laboratories or those that are theoretically predicted in field-free regions. What follows from this is an understanding of the nature of dark matter in terms of currently known physics using particles without a need for particles beyond the standard model. GQM also introduces important new requirements for modelling galaxy formation from supermassive black holes formed at the last phase transition and the subsequent evolution of galaxy structure. It provides an understanding of the origin and quenching of star-forming material, the origin of GCs and their relationship with dSph galaxies and primordial halos, the origin of the satellite galaxies required by LCDM, and the origin of galactic centre black holes and the mass correlations they have with their host galaxies. Taken together, this would suggest that GQM is as fundamentally necessary to include in understanding the nature of the cosmos as is general relativity. Ultimately, the test of any theory is how well it describes future observations, and it is necessary to devise observations to detect the predicted H_2 in dark matter-dominated low-temperature halos.

Funding: This research received no external funding.

Institutional Review Board Statement: Not applicable.

Informed Consent Statement: Not applicable.

Data Availability Statement: Please contact the author directly for further details on the numerical methods used and data presented.

Conflicts of Interest: The author declares there are no conflict of interest in the research work undertaken by the author and presented here.

Notes

1 More recently, a rudimentary transition energy spectrum for these gravitational eigenstates, somewhat analogous to spectral series for electrons, has been demonstrated.

2 There are many examples of novel macroscopic quantum effects—long-range quantum entanglement, superconductivity and superconducting quantum interference, and Bose–Einstein quantum states.

3 The terms “dark particle,” “dark matter,” and “particle darkness” are taken to mean both non-radiative and optically weak interaction.

References

1. Nesvizhevsky, V.V.; Börner, H.G.; Petukhov, A.K.; Abele, H.; Baeßler, S.; Rueß, F.J.; Stöferle, T.; Westphal, A.; Gagarski, A.M.; Petrov, G.A.; et al. Quantum states of neutrons in the Earth's gravitational field. *Nature* **2002**, *415*, 297–299. [CrossRef] [PubMed]
2. Nesvizhevsky, V.V.; Börner, H.G.; Gagarski, A.M.; Petoukhov, A.K.; Petrov, G.A.; Abele, H.; Baeßler, S.; Divkovic, G.; Rueß, F.J.; Stöferle, T.; et al. Measurement of quantum states of neutrons in the Earth's gravitational field. *Phys. Rev. D* **2003**, *67*, 102002. [CrossRef]
3. Jenke, T.; Geltenbort, P.; Lemmel, H.; Abele, H. Realization of a gravity-resonance-spectroscopy technique. *Nat. Phys.* **2011**, *7*, 468–472. [CrossRef]
4. Jenke, T.; Abele, H. Experiments with Gravitationally-bound Ultracold Neutrons at the European Spallation Source ESS. *Phys. Procedia Sci.* **2014**, *51*, 67–72. [CrossRef]
5. Schulz, B. Review on the quantization of gravity. *arXiv* **2014**, arXiv:1409.7977. [CrossRef]
6. Huggett, N.; Matsubara, K.; Wuthrich, C. (Eds.) *Beyond Spacetime, the Foundations of Quantum Gravity*; Cambridge University Press: Cambridge, UK, 2020; ISBN 110847702X/9781108477024.
7. Doran, C.; Lazenby, A.; Dolan, S.; Hinder, I. Fermion absorption cross section of a Schwarzschild black hole. *Phys. Rev. D* **2005**, *71*, 124020. [CrossRef]
8. Vachaspati, T. Schrödinger picture of quantum gravitational collapse. *Class. Quantum Gravity* **2009**, *26*, 215007. [CrossRef]
9. Gossel, G.H.; Berengut, J.C.; Flambaum, V.V. Energy levels of a scalar particle in a static gravitational field close to the black hole limit. *Gen. Relativ. Gravit.* **2011**, *43*, 2673–2683. [CrossRef]
10. Klein, O.; Nishina, Y. On the Scattering of Radiation by Free Electrons According to Dirac's New Relativistic Quantum Dynamics. In *The Oskar Klein Memorial Lectures*; Ekspong, G., Ed.; Original in Z. Phys. 52, 853 (1929); translated from the German by Dr Lars Bergström; World Scientific: Singapore, 2014; Volume 2, pp. 253–272. [CrossRef]
11. Fröwis, F.; Sekatski, P.; Dür, W.; Gisin, N.; Sangouard, N. Macroscopic quantum states: Measures, fragility, and implementations. *Rev. Mod. Phys.* **2018**, *90*, 025004. [CrossRef]
12. Ernest, A.D. Gravitational eigenstates in weak gravity: I. Dipole decay rates of charged particles. *J. Phys. A Math. Theor.* **2009**, *42*, 115207. [CrossRef]
13. Ernest, A.D. Gravitational eigenstates in weak gravity: II. Further approximate methods for decay rates. *J. Phys. A Math. Theor.* **2009**, *42*, 115208. [CrossRef]
14. Ernest, A.D. A Quantum approach to dark matter. In *Dark Matter: New Research*, 1st ed.; Val Blain, J., Ed.; NOVA Science Publishers: New York, NY, USA, 2006; pp. 91–147. ISBN 1-59454-549-9.
15. Bullock, J.S.; Boylan-Kolchin, M. Small-Scale Challenges to the ΛCDM Paradigm. *Annu. Rev. Astron. Astrophys.* **2017**, *55*, 343–387. [CrossRef]
16. Ernest, A.D. Gravitational Quantization and Dark Matter. In *Advances in Quantum Theory*, 1st ed.; Cotaescu, I., Ed.; IntechOpen Ltd.: London, UK, 2011; pp. 221–248. ISBN 978-953-51-0087-4.
17. Ernest, A.D.; Collins, M.P. Structural features of high-n gravitational eigenstates. *Gravit. Cosmol.* **2012**, *18*, 242–248. [CrossRef]
18. Whinray, T.A.; Ernest, A.D. Relations between Transition Rates and Quantum Numbers in Gravitational Potentials. *Gravit. Cosmol.* **2018**, *24*, 97–102. [CrossRef]
19. Ernest, A.D.; Collins, M.P. Halo formation and evolution: Unification of structure and physical properties. In Proceedings of the International Astronomical Union, IAU XXIX General Assembly, Honolulu, HI, USA, 3–14 August 2015; Cambridge University Press: Cambridge, UK, 2015; Volume 11, pp. 298–299. Available online: https://researchoutput.csu.edu.au/en/publications/halo-formation-and-evolution-unification-of-structure-and-physica (accessed on 20 June 2023). [CrossRef]
20. Cawood, C. Globular Clusters and Dwarf Spheroidal Galaxies in the Quantum Dark Matter Scenario: Is There a Connection? Hons. Thesis, Charles Sturt University, Wagga Wagga, Australia, October 2021.
21. Firth, J. State Lifetimes and Spontaneous Emission Rates of Large n, l Eigenstates for a Proton-like Particle in the Infinite Spherical Well. Hons. Thesis, Charles Sturt University, Wagga Wagga, Australia, October 2022.
22. Schiff, L.I. *Quantum Mechanics*, 3rd ed.; McGraw-Hill: New York, NY, USA, 1968.
23. Ernest, A.D. Can quantum theory explain dark matter? In Proceedings of the IAU Symposium: Dark Matter in Galaxies, ASP Conference Series, Sydney, Australia, 21–25 July 2003; Ryder, S.D., Pisano, D.J., Walker, M.A., Freeman, K.C., Eds.; International Astronomical Union. Cambridge University Press: Cambridge, UK, 2004; Volume 220, pp. 497–498, ISBN 9781583811672. [CrossRef]
24. Su, B.-Y.; Li, N.; Feng, L. An inflation model for massive primordial black holes to interpret the JWST observations. *arXiv* **2023**, arXiv:2306.05364. [CrossRef]
25. Carr, B.J. The primordial black hole mass spectrum. *Astrophys. J.* **1975**, *201*, 1–19. [CrossRef]
26. Carr, B.J. Some cosmological consequences of primordial black-hole evaporations. *Astrophys. J.* **1976**, *206*, 8–25. [CrossRef]
27. Carr, B.J. Primordial Black Holes as a Probe of Cosmology and High Energy Physics. *arXiv* **2003**, arXiv:astro-ph/0310838. [CrossRef]
28. Jedamzik, K.; Niemeyer, J.C. Dynamics of primordial black hole formation. *Phys. Rev. D* **1999**, *59*, 124013. [CrossRef]
29. Afshordi, N.; McDonald, P.; Spergel, D.N. Primordial Black Holes as Dark Matter: The Power Spectrum and Evaporation of Early Structures. *Astrophys. J.* **2003**, *594*, L71–L74. [CrossRef]

30. Pospelov, M.; Pradler, J. Big Bang Nucleosynthesis as a Probe of New Physics. *Annu. Rev. Nucl. Part. Sci.* **2010**, *60*, 539–568. [CrossRef]
31. Hu, W.; Dodelson, S. Cosmic Microwave Background Anisotropies. *Annu. Rev. Astron. Astrophys.* **2002**, *40*, 171–216. [CrossRef]
32. Ernest, A.D.; Collins, M.P. The formation and evolution of dark matter halos early in cosmic history. In Proceedings of the IAU General Assembly, Honolulu, HI, USA, 3–14 August 2015; Available online: https://ui.adsabs.harvard.edu/abs/2015IAUGA..2256032E/abstract (accessed on 20 June 2023).
33. Keller, B.W.; Munshi, F.; Trebitsch, M.; Tremmel, M. Can Cosmological Simulations Reproduce the Spectroscopically Confirmed Galaxies Seen at z $\geq$ 10? *Astrophys. J. Lett.* **2023**, *943*, L28. [CrossRef]
34. Williams, H.; Kelly, P.L.; Chen, W.; Brammer, G.; Zitrin, A.; Treu, T.; Scarlata, C.; Koekemoer, A.M.; Oguri, M.; Lin, Y.H.; et al. A magnified compact galaxy at redshift 9.51 with strong nebular emission lines. *Science* **2023**, *380*, 416–420. [CrossRef]
35. Reardon, D.J.; Zic, A.; Shannon, R.M.; Hobbs, G.B.; Bailes, M.; Di Marco, V.; Kapur, A.; Rogers, A.F.; Thrane, E.; Askew, J.; et al. Search for an Isotropic Gravitational-wave Background with the Parkes Pulsar Timing Array. *Astrophys. J. Lett.* **2023**, *951*, L6. [CrossRef]
36. Fields, B.D. The Primordial Lithium Problem. *Annu. Rev. Nucl. Part. Sci.* **2011**, *61*, 47–68. [CrossRef]
37. Bassett, B.A.; Hlozek, R. Baryon acoustic oscillations. *arXiv* **2009**, arXiv:0910.5224. [CrossRef]
38. Hodges-Kluck, E.J.; Miller, M.J.; Bregman, J.N. The rotation of hot gas around the Milky Way. *Astrophys. J.* **2016**, *822*, 21. [CrossRef]
39. Carroll, B.W.; Ostlie, D.A. *An Introduction to Modern Astrophysics*, 2nd ed.; Pearson Addison Wesley: Boston, MA, USA, 2020; pp. 960–961. ISBN 0-8053-0402-9.
40. Yıldırım, A.; van den Bosch, R.C.; van de Ven, G.; Husemann, B.; Lyubenova, M.; Walsh, J.L.; Gebhardt, K.; Gültekin, K. MRK 1216 and NGC 1277—An orbit-based dynamical analysis of compact, high-velocity dispersion galaxies. *Mon. Not. R. Astron. Soc.* **2015**, *452*, 1792–1816. [CrossRef]
41. Schwarwachter, J.; Combes, F.; Salome, P.; Sun, M.; Krips, M. The overmassive black hole in NGC 1277: New constraints from molecular gas kinematics. *Mon. Not. R. Astron. Soc.* **2016**, *457*, 4272–4284. [CrossRef]
42. Mancera Piña, P.E.; Fraternali, F.; Oosterloo, T.; Adams, E.A.; Oman, K.A.; Leisman, L. No need for dark matter: Resolved kinematics of the ultra-diffuse galaxy AGC 114905. *Mon. Not. R. Astron. Soc.* **2021**, *512*, 3230–3242. [CrossRef]
43. Kalberla, P.M.W.; Kerp, J.; Haud, U. HI filaments are cold and associated with dark molecular gas. *Astron. Astrophys.* **2020**, *639*, A26. [CrossRef]
44. Simon, J.D. The Faintest Dwarf Galaxies. *Annu. Rev. Astron. Astrophys.* **2019**, *57*, 375–415. [CrossRef]
45. Stegmann, J.; Capelo, P.R.; Bortolo, E.; Mayer, L. Improved constraints from ultra-faint dwarf galaxies on primordial black holes as dark matter. *Mon. Not. R. Astron. Soc.* **2020**, *492*, 5247–5260. [CrossRef]
46. Bowman, J.D.; Rogers, A.E.E.; Monsalve, R.A.; Mozdzen, T.J.; Mahesh, N. An absorption profile centred at 78 megahertz in the sky-averaged spectrum. *Nature* **2018**, *555*, 67–70. [CrossRef] [PubMed]
47. Kurth, W.S.; Gurnett, D.A. Observations of a Radial Density Gradient in the Very Local Interstellar Medium by Voyager 2. *Astrophys. J. Lett.* **2020**, *900*, L1. [CrossRef]
48. de Avillez, M.A.; Anela, G.J.; Asgekar, A.; Breitschwerdt, D.; Schnitzeler, D.H. Electrons in the supernova-driven interstellar medium. *Astron. Astrophys.* **2020**, *644*, A156. [CrossRef]